

## Steady flow in a helically symmetric pipe

By L. ZABIELSKI AND A. J. MESTEL

Mathematics Department, Imperial College, 180 Queen's Gate London SW7 2BZ, UK

(Received 13 March 1997 and in revised form 27 October 1997)

Fully developed flow in an infinite helically coiled pipe is studied, motivated by physiological applications. Most of the bends in the mammalian arterial system curve in a genuinely three-dimensional way, so that the arterial centreline has not only curvature but torsion and can be modelled by a helix. Flow in a helically symmetric pipe generalizes related problems in axisymmetry (Dean flow) and two-dimensionality, but the geometry ensures that even irrotational flow has a cross-pipe component. Fully developed helical flows driven by a steady pressure gradient are studied analytically and numerically. Varying the radius and pitch of the helical pipe, the effects of curvature and torsion on the flow are investigated.

---

### 1. Introduction

The motion of fluids down pipes is a fundamental and much-studied problem. The engineering applications are manifest, as evident from the review article by Berger, Talbot & Yao (1983). This paper is particularly motivated by studies of blood flow in the body, an essential introduction to which is given by Pedley (1980). In engineering applications the flow is often turbulent, but in the circulatory systems of humans and smaller mammals it is nearly always laminar. However, the physiological geometry is highly complex with a multitude of bends and bifurcations. In addition, the flow is driven by the pumping action of the heart, which has a complex periodic time dependence. In this paper steady flows are investigated, while pulsatile flows are considered in the contiguous paper Zabielski & Mestel (1998), henceforth referred to as ZM2. Other possible complications include the arterial wall distensibility and the weakly non-Newtonian behaviour of blood at low shear rates. Such effects will not be considered in the present works.

If a straight pipe carrying a steady, uni-directional flow is uniformly bent into a portion of a torus, variations in the centripetal acceleration set up a cross-pipe pressure gradient which drives a so-called secondary flow. Theoretical studies of steady flow in curved pipes began with Dean (1927, 1928). If the curvature of the pipe is small, then the flow depends on a single parameter, the Dean number, which is a Reynolds number modified by curvature. The cross-pipe flow consists of two symmetric recirculating regions. As the Dean number is increased an asymptotic structure appears, with a core flow dependent only on distance from the axis of the torus. Boundary layers begin at the outer wall and travel towards the inner wall, where the scalings break down (Smith 1976). To date, a self-consistent picture for the high Dean number limit has not been presented (Dennis & Riley 1991).

Numerical solutions of the Dean problem have also been calculated (Collins & Dennis 1975). At moderately large Dean number multiple solutions have been found (Dennis & Ng 1982; Daskopoulos & Lenhoff 1989), with four recirculating regions rather than two. However, most if not all of these are unstable when steadiness and

top-bottom symmetry are not imposed (Yanase, Goto & Yamamoto 1989). All these studies have considered the low-curvature Dean problem. A four-vortex solution has been observed by Cheng & Mok (1986) for an experiment with larger curvature.

In the body and in other practical problems, the pipe curvature is far from small. In addition, the curvature is frequently non-planar, so that the pipe centreline is a curve with *torsion* as well as curvature (Caro *et al.* 1996). The simplest such curve is a helix. In this paper and ZM2, the flow inside a helical pipe is investigated. The pipe is considered to have infinite extent, so that helical symmetry can be imposed on the solution, essentially reducing the problem to two dimensions. Arbitrary constant curvature and torsion are permitted, so that a particular arterial bend can be modelled by appropriate values. The twisted artery in an umbilical cord can thus be very well represented. In general, it is assumed that the flow in an infinite helical pipe will approximate conditions in a curved artery of finite extent. Such an assumption involves the neglect of first, entrance effects and secondly, the influence of the time-dependent flow component. The latter assumption is dubious in the aorta, a large blood vessel close to the heart, where the driving pressure gradient is far from steady (Chandran 1993). Even during diastole, the second part of the cardiac cycle when the pressure gradient is more or less uniform, a fully developed flow for which viscosity is given a long time to act is unlikely to be an accurate representation. It may well be that the rapid interactions between pressure gradient and the three-dimensional geometry are better reflected by the inertially dominated flows considered in §3. At some distance from the heart, however, the pressure pulse becomes more uniform in time and a steady flow is a plausible approximation. Steady flow in nearly straight pipes with non-uniform curvature and torsion is being studied by Gammack & Hydon (1998).

From a medical point of view, the problem is important to the understanding and prevention of atherosclerosis and related conditions. Physiologists regard the circulatory system as being of optimal design, and hence the existence of three-dimensional bends, even when there is no obvious logistical reason for them, suggests some evolutionary advantage should derive from such configurations. Caro, Fitzgerald & Schroter (1971) suggested that regions of the arterial wall where the fluid shear is low are prime candidates for sites of the formation of atherosclerotic lesions, and this is now generally accepted (Giddens, Zarins & Glagov 1993; Pedley 1995). The enhanced cross-pipe flows which occur in non-planar bends may thus help to prevent atheroma. A further possible advantage to such bends is the inhibition of separation, as discussed in ZM2.

Helical symmetry is a natural conjunction of two-dimensional and axisymmetric symmetries, but has confusing properties. Genuine helical symmetry can be defined for  $O(1)$  curvature and torsion (Childress, Landman & Strauss 1989; Landman 1990 and Dritschel 1991). A streamfunction for the cross-pipe flow occurs naturally, although care must be taken in interpreting the cross-section. However, for small curvature and torsion an alternative representation is possible using an orthogonal coordinate system introduced by Germano (1982). Some confusion has resulted from the use of these coordinates which do not permit a streamfunction description. As a result, different representations of the same solution have not always been recognized. Tuttle (1990) and Liu & Masliyah (1993) have reconciled many of the apparent discrepancies, but there seems little attraction to this approach rather than the global formulation described below.

The above problems and other implications of helical symmetry are discussed in §2 of this paper. In §3, the governing equations are derived and exact solutions for a rectangular boundary are found for potential type flows. In §4, a numerical approach is

described. At high Reynolds numbers a structure similar to that of the Dean problem evolves, with the same unresolved behaviour at the inner wall. Some hint of a possible inertial region with closed streamlines is discernible from the numerics. At intermediate Reynolds numbers, the cross-pipe flow may consist of either one or two vortices. The latter structure has low-shear regions associated with the stagnation points.

No non-uniqueness of the steady helical solutions was found. This is consistent with the discussion of Yanase *et al.* (1989) because the numerical method described in §4 imposes neither a steady state nor top/bottom symmetry. Hence only solutions stable to all helically symmetric disturbances can be obtained.

## 2. Helical symmetry

Most known solutions of the Navier–Stokes equations have some kind of spatial symmetry. If the surfaces on which boundary conditions must be satisfied are invariant with respect to a given group of isometric transformations, the same spatial invariance can often be imposed on the velocity field and the governing equations can be simplified. Familiar cases are axisymmetric and two-dimensional flows, which are invariant respectively to the rotation group (around, say, the  $z$ -axis) and the translation group (in, say, the  $z$ -direction). Helical geometries can be regarded as the superposition of such rotation and translation. A single parameter,  $\varepsilon$ , relating the distance in the  $z$ -direction and the rotation angle determines a particular helical symmetry, so that during rotation through  $2\pi$  the  $z$ -coordinate advances through  $2\pi/\varepsilon$ . A helical transformation defined in this way is isometric and defines uniquely a symmetry direction  $\mathbf{H}$  as the tangent vector field to the family of helical curves with the same constant pitch  $\varepsilon$ . In terms of cylindrical coordinates  $(r, \theta, z)$ ,  $\mathbf{H}$  can be expressed as

$$\mathbf{H} = \frac{1}{h^2}(-\varepsilon r \mathbf{e}_\theta + \mathbf{e}_z), \quad \text{where } h^2 = 1 + \varepsilon^2 r^2. \quad (2.1)$$

Throughout this paper  $\mathbf{e}$  denotes a unit vector in the direction of the suffix. A scalar function  $f$  is called helically symmetric if it does not vary in the  $\mathbf{H}$ -direction, so that  $\mathbf{H} \cdot \nabla f = 0$ . As expected, in the limiting cases helical symmetry reduces to two-dimensionality and axisymmetry:

$$\lim_{\varepsilon \rightarrow 0} \mathbf{H} = \mathbf{e}_z, \quad \lim_{\varepsilon \rightarrow \infty} h\mathbf{H} = -\mathbf{e}_\theta.$$

The vector  $\mathbf{H}$  is a non-unit vector ( $\mathbf{e}_H = h\mathbf{H}$ ) and has been normalized to be a Beltrami field, so that

$$\mathbf{H} \parallel \nabla \times \mathbf{H}. \quad (2.2)$$

This, together with the fact that  $\mathbf{H}$  is solenoidal ( $\nabla \cdot \mathbf{H} = 0$ ) implies that the vector field  $\mathbf{H}$  itself satisfies the steady Euler equation of motion.

Two other vectors need to be chosen in order to obtain a complete orthogonal set. One of them can be taken as  $\mathbf{e}_r$  (since  $\mathbf{H} \cdot \mathbf{e}_r = 0$ ) and then the third is determined by the cross-product

$$\mathbf{e}_\phi = h\mathbf{H} \times \mathbf{e}_r = \frac{1}{h}(\mathbf{e}_\theta + \varepsilon r \mathbf{e}_z).$$

The system  $(\mathbf{e}_r, \mathbf{e}_\phi, \mathbf{H})$  forms an orthogonal helical vector base (compare Childress *et al.* 1989; Dritschel 1991; and Landman 1990) and

$$\left. \begin{aligned} \nabla \times \mathbf{e}_r &= 0, & \nabla \cdot \mathbf{e}_r &= r^{-1}, \\ \nabla \times \mathbf{e}_\phi &= (rh)^{-1} \mathbf{H}, & \nabla \cdot \mathbf{e}_\phi &= 0, \\ \nabla \times \mathbf{H} &= -2\varepsilon h^{-2} \mathbf{H}, & \nabla \cdot \mathbf{H} &= 0. \end{aligned} \right\} \quad (2.3)$$

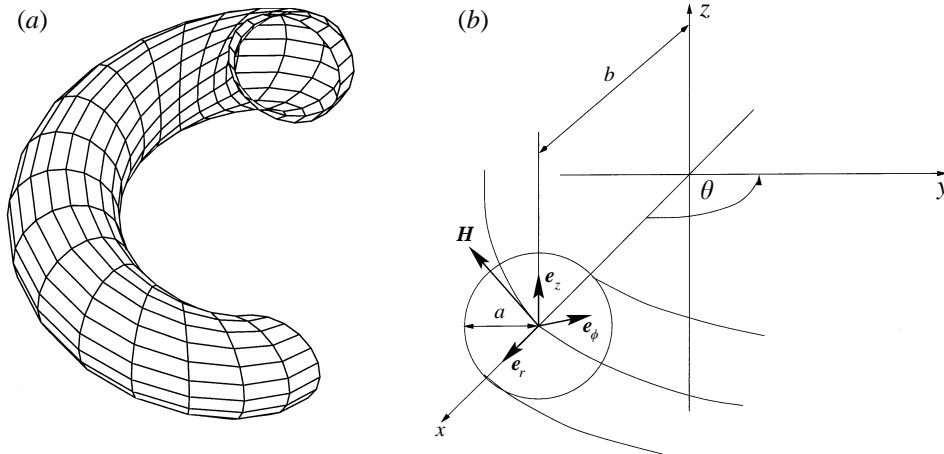


FIGURE 1. (a) A circular pipe ( $\varepsilon = 1$ ) and (b) Helical coordinates related to cylindrical polars. The vector  $\mathbf{H}$  points in the local symmetry direction, and helically symmetric functions depend only on  $r$  and  $\phi = \theta + \varepsilon z$ .

An interesting fact is that the Beltrami property (2.2) of the helical vector  $\mathbf{H}$  does not allow a transformation of variables that would define an orthogonal helical coordinate system. From (2.3), the vectors  $\mathbf{e}_\phi$  and  $\mathbf{H}$  have non-zero curl. For  $\mathbf{e}_\phi$  there exists a function  $f(r) = h/r$  such that  $\nabla \times (f\mathbf{e}_\phi) = 0$  and this defines a new coordinate  $\phi = \theta + \varepsilon z$ . A unique representation occurs if  $\phi$  is restricted to the range  $0 \leq \phi < 2\pi$ . However, in the case of  $\mathbf{H}$ , using (2.3),

$$\nabla \times f\mathbf{H} = \nabla f \times \mathbf{H} + f(-2\varepsilon h^{-2})\mathbf{H} \quad (2.4)$$

and

$$\nabla \times f\mathbf{H} = 0 \Rightarrow \mathbf{H} \cdot \nabla \times f\mathbf{H} = 0 \Rightarrow f(-2\varepsilon h^{-2})\mathbf{H} \cdot \mathbf{H} = 0 \Rightarrow f = 0.$$

Geometrically this means that the field of planes normal to the vector  $\mathbf{H}$  is not integrable, so that one cannot find a surface to which all these planes are tangent. In general, a condition for such integrability is given by the Frobenius theorem (e.g. Arnold 1983).

All helically symmetric functions depend only on  $r$  and  $\phi$  so the lack of a third coordinate is not so inconvenient. However, this may cause difficulties should the symmetry assumption be relaxed which might necessitate the use of non-orthogonal coordinates.

Helical coordinates are sketched in figure 1 along with a helical pipe of circular cross-section, as defined below. In this paper we will consider problems with left-handed helices for which  $\varepsilon > 0$ . These are clearly isomorphic to cases with  $\varepsilon < 0$ .

For a given vector field, say  $\mathbf{u}$ , the following transformation formulae hold:

$$\begin{pmatrix} \mathbf{e}_r \\ \mathbf{e}_\phi \\ \mathbf{H} \end{pmatrix} = \begin{bmatrix} 1 & 0 & 0 \\ 0 & 1/h & \varepsilon r/h \\ 0 & -\varepsilon r/h^2 & 1/h^2 \end{bmatrix} \begin{pmatrix} \mathbf{e}_r \\ \mathbf{e}_\theta \\ \mathbf{e}_z \end{pmatrix} \Rightarrow \begin{cases} u_r = u_r \\ u_\theta = (1/h) u_\phi - (\varepsilon r/h^2) v \\ u_z = (\varepsilon r/h) u_\phi + (1/h^2) v, \end{cases} \quad (2.5)$$

where  $(u_r, u_\theta, u_z)$  and  $(u_r, u_\phi, v)$  are the components of  $\mathbf{u}$  in, respectively, cylindrical and helical coordinates. From (2.5), one can deduce in particular that

$$\nabla = \mathbf{e}_r \frac{\partial}{\partial r} + \mathbf{e}_\phi \frac{h}{r} \frac{\partial}{\partial \phi}.$$

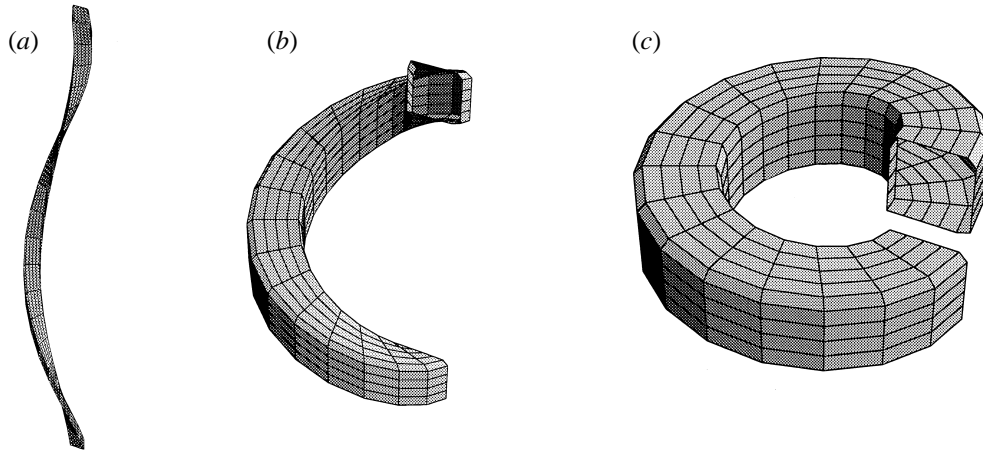


FIGURE 2. Rectangular helical pipes (a)  $\epsilon = 0.1$ , (b) 1, (c) 10. Two-dimensionality and axisymmetry are approached as  $\epsilon \rightarrow 0, \infty$  respectively.

The vector field  $\mathbf{u}$  is helically symmetric when all its components,  $(u_r, u_\phi, v)$ , are helically symmetric. If additionally  $\mathbf{u}$  is divergence-free, as for incompressible flows, then it can be written

$$\mathbf{u} = \mathbf{H} \times \nabla \Psi + v \mathbf{H}, \tag{2.6}$$

where  $\Psi = \Psi(r, \phi)$  is a helical streamfunction. The vorticity  $\boldsymbol{\omega} = \nabla \times \mathbf{u}$  can then be expressed as

$$\boldsymbol{\omega} = \nabla v \times \mathbf{H} + \xi \mathbf{H} \tag{2.7}$$

with

$$\mathcal{L}\Psi = \xi + \frac{2\epsilon}{h^2}v, \quad \text{where} \quad \mathcal{L} = \frac{h^2}{r} \frac{\partial}{\partial r} \left( \frac{r}{h^2} \frac{\partial}{\partial r} \right) + \frac{h^2}{r^2} \frac{\partial^2}{\partial \phi^2}. \tag{2.8}$$

### 2.1. Helical pipes

A helical pipe can be defined when a closed contour,  $S$ , is specified in the  $(r, \phi)$ -plane and then translated by  $\mathbf{H}$ . This contour essentially determines the pipe cross-section which, however, may not have exactly the same shape in physical space. A convenient representation is to associate  $S$  with the zero level curve of some helically symmetric function

$$S : F(r, \phi) = 0.$$

Note that a pipe constructed in this way does not have a simple cross-section corresponding to the helical decomposition of a velocity field. Usually one would take a plane normal to the direction of the pipe and consider the flow field as a superposition of the flow down the pipe and the two-dimensional flow in the cross-section. In the case of helical symmetry, however, such a cross-sectional plane (or even surface) would have a normal in the  $\mathbf{H}$ -direction which is not possible from (2.4). Nevertheless, decomposition of the flow field is possible as in (2.6) but instead of the normal cross-section in physical space one has to refer to the flow in the parametric  $(r, \phi)$ -plane together with the component in the helical direction.

Pipes defined by a rectangular  $S$  in the  $(r, \phi)$ -plane also have rectangular cross-sections in physical space ( $\theta = 0$  say), and the effect of varying  $\epsilon$  is shown in figure 2. Circular pipes are not so straightforward.

## 2.1.1. Circular pipes

For pipes at some distance from the  $z$ -axis, a circular or elliptical contour in  $(r, \phi)$  variables is mapped onto an approximately elliptical shape in physical space. Thus it is possible to choose the axes of such an ellipse to give a nearly circular image. However, while this parametrization is reasonable for large values of  $r$  and moderate  $\varepsilon$ , the deformation of the circle becomes more pronounced close to the  $z$ -axis for small  $\varepsilon$  (a cusp-like shape is formed) which renders such a description unsuitable. Thus, in the present work, a circular pipe is defined first by fixing its centreline to be a helix of pitch  $\varepsilon$  on the cylinder  $r = b$ , and then by taking a circle in the plane orthogonal to this helix. The direction of the centreline is denoted by  $\mathbf{H}_b = \mathbf{H}|_{r=b}$ , and  $h_b = (1 + \varepsilon^2 b^2)^{1/2}$ . Polar coordinates  $(\rho, \eta)$  in the  $\mathbf{H}_b$ -plane with origin on the centreline are introduced so that the pipe is given by  $\rho = 1$ . Then it is not difficult to show that

$$\left. \begin{aligned} r &= \left( (\rho \cos \eta + b)^2 + \frac{\rho^2}{h_b^2} \sin^2 \eta \right)^{1/2}, \\ \phi &= \arctan \left( \frac{\rho \sin \eta}{h_b(\rho \cos \eta + b)} \right) + \frac{\varepsilon^2 b}{h_b} \rho \sin \eta. \end{aligned} \right\} \quad (2.9)$$

Interpreting the arctangent appropriately, this defines a coordinate transformation,  $\mathcal{T}$ ,

$$\mathcal{T} : [0, \infty) \times [0, 2\pi) \ni (r, \phi) \longrightarrow (\rho, \eta) \in [0, \infty) \times (-\pi, \pi].$$

As  $\varepsilon \rightarrow \infty$  it follows from (2.9) that  $(r, \phi/\varepsilon) \rightarrow (\rho \cos \eta + b, \rho \sin \eta)$  which coincides with the studies in axisymmetry, e.g. Dean (1928).

A vector base  $(\mathbf{e}_\rho, \mathbf{e}_\eta, \mathbf{H})$ , corresponding to the  $(\rho, \eta)$  coordinates, can also be found. The radial vector  $\mathbf{e}_\rho = \nabla \rho$  and so  $\mathbf{e}_\eta$  is determined by

$$\mathbf{e}_\eta = h\mathbf{H} \times \mathbf{e}_\rho.$$

This leads to the following formula for the gradient:

$$\nabla = \mathbf{e}_\rho \frac{\partial}{\partial \rho} + \mathbf{e}_\eta \frac{h}{r} \left| \frac{\partial(\rho, \eta)}{\partial(r, \phi)} \right| \frac{\partial}{\partial \eta}. \quad (2.10)$$

The first derivative of the transformation  $\mathcal{T}$  can be obtained by differentiating (2.9):

$$D\mathcal{T} = \frac{1}{h_b^2 r^2} \begin{bmatrix} r(h_b^2 \cos \eta (b + \rho \cos \eta) + \rho \sin^2 \eta) & -\rho b r \sin \eta (h_b^2 + \rho b \varepsilon^2 \cos \eta) \\ h_b b h^2 \sin \eta & h_b \rho (\rho + b h^2 \cos \eta) \end{bmatrix} \quad (2.11)$$

and hence the Jacobian  $J = |\partial(r, \phi)/\partial(\rho, \eta)|$  is given by

$$J = \frac{\rho}{2h_b^3 r^3} (\rho^2 + \rho^2 h_b^2 + 2b^2 h^2 h_b^2 + 2\rho b h_b^2 \cos \eta (1 + h^2) + \rho^2 b^2 \varepsilon^2 \cos(2\eta)). \quad (2.12)$$

Based on (2.10)–(2.12) most of the differential expressions in the governing equations can easily be transformed into  $(\rho, \eta)$  variables and only the terms where elements of the Hessian of  $\mathcal{T}$  appear require more effort. The operator  $\mathcal{L}$  in (2.8) takes the form

$$\mathcal{L} = \frac{\partial^2}{\partial \rho^2} + \frac{h^2}{r^2 J^2} \frac{\partial^2}{\partial \eta^2} + (\mathcal{L}\rho) \frac{\partial}{\partial \rho} + (\mathcal{L}\eta) \frac{\partial}{\partial \eta},$$

where  $\mathcal{L}\rho = h^2 \nabla \cdot (h^{-2} \mathbf{e}_\rho)$ ,  $\mathcal{L}\eta = h^2 \nabla \cdot [\mathbf{e}_\eta / (hrJ)]$  can also be obtained in closed form (see the Appendix).

2.2. Comments on alternative coordinate systems

In a number of papers (recently Liu & Masliyah 1993; Tuttle 1990; Germano 1989; and Kao 1987) steady, fully developed flow inside a circular, helical pipe has been studied using an orthogonal coordinate system which was first introduced by Germano (1982). Germano's coordinates rely essentially on the Frenet triad of unit vectors associated with the pipe centreline.

Defining the centreline with the position vector  $\mathbf{R}(l)$ , where  $l$  is the natural parameter (arclength), the position vector  $\mathbf{r}$  of a nearby point can be expressed in terms of the tangent, normal and binormal vectors,  $\mathbf{T}$ ,  $\mathbf{N}$  and  $\mathbf{B}$  as

$$\mathbf{r} = \mathbf{R}(l) + x\mathbf{N}(l) + y\mathbf{B}(l).$$

A given point in physical space is thus determined by  $l$  and  $(x, y)$  Cartesian coordinates in a cross-sectional plane. Unfortunately, when the centreline is a helix of radius  $b$  and pitch  $\varepsilon$ , these form a non-orthogonal system. The (contravariant) vectors  $\mathbf{N}$  and  $\mathbf{B}$  do not vary over a plane of constant  $l$  to which the (covariant)  $\mathbf{T}$  is normal. It must, however, be emphasized that  $\mathbf{T}$  does not point in the direction of an  $l$ -line if  $x$  and  $y$  are constant but non-zero. As observed by Germano, orthogonal coordinates in a reference frame rotating with respect to  $\mathbf{N}$  and  $\mathbf{B}$  can be used instead. In either case the description is local, valid only when  $a < 1/\kappa$ , where  $a = 1$  is the pipe radius and  $\kappa = \varepsilon^2 b/h_b^2$  the curvature. This condition does not permit strongly curved pipes.

The entire analysis is based on the assumption of helically symmetric motion. In Germano's approach it is assumed that the fully developed flow does not depend on  $l$ . Hence, the symmetry direction,  $\mathbf{s}$ , takes the form

$$\mathbf{s} = \frac{\partial \mathbf{r}}{\partial l} = \mathbf{T} + x(-\kappa\mathbf{T} + \tau\mathbf{B}) + y(-\tau\mathbf{N}) \tag{2.13}$$

using the Frenet formulae, where  $\tau = -\varepsilon/h_b^2$  is the torsion. Parametrizing the helix explicitly, it can be shown that  $r^2 = (b-x)^2 + y^2/h_b^2$  and that  $\mathbf{T}, \mathbf{N}, \mathbf{B}$  are related to the cylindrical polar vectors at a given point by

$$\begin{pmatrix} \mathbf{T} \\ \mathbf{N} \\ \mathbf{B} \end{pmatrix} = \begin{bmatrix} \varepsilon by/(h_b^2 r) & -\varepsilon b(b-x)/(h_b r) & 1/h_b \\ -(b-x)/r & -y/(h_b r) & 0 \\ y/(h_b^2 r) & -(b-x)/(h_b r) & -\varepsilon b/h_b \end{bmatrix} \begin{pmatrix} \mathbf{e}_r \\ \mathbf{e}_\theta \\ \mathbf{e}_z \end{pmatrix}. \tag{2.14}$$

In particular, on the centreline  $x = y = 0$  this gives  $\mathbf{T} = \mathbf{e}_H$ ,  $\mathbf{N} = -\mathbf{e}_r$  and  $\mathbf{B} = -\mathbf{e}_\theta$ . Substituting the transformation formulae (2.14) into (2.13) yields

$$\mathbf{s} = \frac{1}{h_b}(-\varepsilon r \mathbf{e}_\theta + \mathbf{e}_z) = \frac{h^2}{h_b^2} \mathbf{H}. \tag{2.15}$$

Hence whenever the curvature of the pipe is small, and the  $(l, x, y)$  description is possible, the vectors  $\mathbf{s}$  and  $\mathbf{H}$  are parallel and the symmetry direction of the Germano approach is identical to that of the present work. Using (2.5) and (2.14) an appropriate transformation between the velocity components can easily be found, showing that the equations of motion used by Germano and others are equivalent to those considered here.

Any coordinate system can be used to represent a given flow, but for helical symmetry there is a natural decomposition of the flow into a primary component, in the symmetry direction  $\mathbf{s} \equiv \mathbf{H}$ , and a secondary motion orthogonal to it. For pipe flows the primary motion is down the pipe while the secondary component is identified with cross-pipe flow. As shown below (2.4), there exists no coordinate system defining a covariant vector field in the direction of  $\mathbf{H}$ . Since contravariant

and covariant components are the same for orthogonal systems, this immediately implies that neither Germano coordinates nor any other orthogonal system yields a vector base containing the symmetry direction  $\mathbf{H}$ . For the non-orthogonal  $(l, x, y)$  coordinates, the covariant and contravariant descriptions differ and the vector field  $\mathbf{T}$  is  $l$ -covariant while  $\mathbf{H}$  is  $l$ -contravariant. Helical symmetry could be represented using  $(x, y)$ -covariant and  $l$ -contravariant vectors. Yet this is an unnatural mixture and previous studies have used either strictly covariant or contravariant systems, with a different down-pipe velocity from that implied by the helical symmetry.

While it is not essential to use the natural decomposition of the flow, such notions as *primary flow* or *secondary motion* are otherwise dependent on definition and the coordinate system in use. Care must then be taken when comparing statements on, for example, the effect of torsion on the secondary motion. As the primary flow tends to be dominant, if a non-canonical decomposition of the velocity field is used, part of this strong flow is included in the cross-sectional motion. This has resulted in some confusion in the literature which was unravelled by Tuttle (1990) who demonstrated the equivalence of the  $(l, x, y)$  and Germano approaches.

The centreline-based formulations give rise to some technical difficulties. Despite the fact that the simplified problem is really two-dimensional, a proper streamfunction cannot be defined, rendering flow description difficult. Moreover, the coordinate system is only defined locally, resulting in an unnecessary restriction of small curvature. In fact, there is nothing fundamental or unique about the centreline curve, as becomes clear when helical pipes with non-circular cross-section are considered. Helical symmetry is a global concept and, as shown in the present work, can be studied in pipes of arbitrary cross-section, curvature and torsion. When the velocity is decomposed in accordance with the symmetry global coordinates can easily be introduced. A helical streamfunction then appears naturally although the flow it represents is not confined to a planar cross-section. This reflects the complexity and genuinely three-dimensional behaviour of helical flows.

In summary, coordinate systems based on the Frenet vector triad associated with the pipe centreline give representations of helical flows formally equivalent to that of the present work. The description is more cumbersome, however, and care must be taken when comparing potentially coordinate-dependent concepts such as secondary and primary motion. The restriction on admissible pipe curvature associated with the local description suggests that there is little attraction to such an approach.

### 3. The governing equations

The laminar motion inside a helical pipe of an incompressible Newtonian fluid, of constant density  $\rho_0$  and kinematic viscosity  $\nu$ , is considered. A steady, helically symmetric flow is possible provided the imposed down-pipe pressure gradient is of the form (compare (3.13) below)

$$h^2 \mathbf{H} \cdot \nabla p = h_b \rho_0 G. \quad (3.1)$$

Here  $h_b = (1 + \varepsilon^2 b^2)^{1/2}$  and  $b$  is a typical distance between the pipe and the  $z$ -axis. The constant  $G$  measures the magnitude of the down-pipe component of the pressure gradient.

The helical decompositions for the velocity and vorticity fields given by (2.6) and (2.7), as shown in Childress *et al.* 1989 and Dritschel (1991), lead to

$$\mathbf{u} \times \boldsymbol{\omega} = \mathbf{H} \cdot (\nabla \Psi \times \nabla v) \mathbf{H} - h^{-2} (\xi \nabla \Psi + v \nabla v) \quad (3.2)$$



and hence

$$\begin{aligned} \nabla \times (\mathbf{u} \times \boldsymbol{\omega}) &= \nabla(\mathbf{H} \cdot (\nabla\Psi \times \nabla v)) \times \mathbf{H} \\ &+ \mathbf{H} \cdot (\nabla\Psi \times \nabla v) \left(-\frac{2\varepsilon}{h^2}\right) \mathbf{H} - \nabla\left(\frac{\xi}{h^2}\right) \times \nabla\Psi + \nabla\left(\frac{v}{h^2}\right) \times \nabla v. \end{aligned} \quad (3.3)$$

Expressions for the viscous terms can be easily obtained from (2.8):

$$\nabla^2 \mathbf{u} = -\nabla \times \boldsymbol{\omega} = \mathbf{H} \times \nabla \xi + \left(\mathcal{L}v + \frac{2\varepsilon}{h^2} \xi\right) \mathbf{H}, \quad (3.4)$$

$$\nabla^2 \boldsymbol{\omega} = -\mathbf{H} \times \nabla \left(\mathcal{L}v + \frac{2\varepsilon}{h^2} \xi\right) + \left(\mathcal{L}\xi - \frac{2\varepsilon}{h^2} \left(\mathcal{L}v + \frac{2\varepsilon}{h^2} \xi\right)\right) \mathbf{H}. \quad (3.5)$$

Substituting (3.1), (3.2), (3.3), (3.4) into the velocity and vorticity equations and taking the scalar product with  $\mathbf{H}$ , one can derive the following:

$$\frac{\partial v}{\partial t} + \mathbf{H} \cdot (\nabla\Psi \times \nabla v) = h_b G + v \left(\mathcal{L}v + \frac{2\varepsilon}{h^2} \xi\right), \quad (3.6)$$

$$\begin{aligned} \frac{\partial \xi}{\partial t} + \mathbf{H} \cdot \left(-\frac{2\varepsilon}{h^2} (\nabla\Psi \times \nabla v) - h^2 \nabla\left(\frac{\xi}{h^2}\right) \times \nabla\Psi - h^2 \nabla\left(\frac{v}{h^2}\right) \times \nabla v\right) \\ = v \left(\mathcal{L}\xi - \frac{2\varepsilon}{h^2} \left(\mathcal{L}v + \frac{2\varepsilon}{h^2} \xi\right)\right). \end{aligned} \quad (3.7)$$

The scalar triple products in (3.6) and (3.7) can be expressed as Jacobians:

$$\mathbf{H} \cdot (\nabla f \times \nabla g) = \frac{1}{r} J(f, g) = \frac{1}{r} \left(\frac{\partial f}{\partial r} \frac{\partial g}{\partial \phi} - \frac{\partial g}{\partial r} \frac{\partial f}{\partial \phi}\right).$$

If  $a$  is a typical pipe radius, and the following scales are introduced:

$$t \sim \frac{a^2}{v}, \quad r \sim a, \quad \frac{\Psi}{a^2}, \quad \frac{v}{a}, \quad \xi \sim \frac{v}{a^2} \quad (3.8)$$

then (3.6) and (3.7) take the non-dimensional forms

$$\frac{\partial v}{\partial t} + \frac{1}{r} J(\Psi, v) = R + \mathcal{L}v + \frac{2\varepsilon}{h^2} \xi, \quad (3.9)$$

$$\frac{\partial \xi}{\partial t} - \frac{2\varepsilon}{h^2} \frac{1}{r} J(\Psi, v) + \frac{1}{r} J(\Psi, \xi) + \frac{2\varepsilon^2}{h^2} \left(\xi \frac{\partial \Psi}{\partial \phi} + v \frac{\partial v}{\partial \phi}\right) = \mathcal{L}\xi - \frac{2\varepsilon}{h^2} \left(\mathcal{L}v + \frac{2\varepsilon}{h^2} \xi\right), \quad (3.10)$$

where the  $\mathbf{H}$ -component of vorticity,  $\xi$ , satisfies the kinematic relation (2.8), repeated here:

$$\mathcal{L}\Psi = \frac{2\varepsilon}{h^2} v + \xi. \quad (3.11)$$

The system of equations (3.9), (3.10) and (3.11), together with suitable solid boundary conditions, determines a general flow with helical symmetry. Such a flow, in addition to the curvature and torsion controlled by  $b$  and  $\varepsilon$ , depends on the parameter

$$R = h_b \frac{Ga^3}{v^2} \quad (3.12)$$

which can be related to the Dean number,  $D$ , by  $R = Dh_b(b/a)^{1/2}$ .

## 3.1. Potential flow with helical symmetry

For irrotational flows, the velocity field can be represented as a gradient of some scalar potential, so that  $\mathbf{u} = \nabla V$ . Such flows are important in slug-like entry problems or, as discussed in ZM2, when the driving pressure gradient is rapidly oscillating, giving rise to a fully developed potential core flow with Stokes boundary layers. If  $\mathbf{u}$  has a component in the  $\mathbf{H}$ -direction, then  $\mathbf{H} \cdot \nabla V \neq 0$  and by definition  $V$  itself cannot be helically symmetric. Let us assume that  $V = V(r, \phi, s)$  where  $s$  is a third coordinate chosen so that every point has a unique representation in terms of  $r, \phi$  and  $s$ . It is convenient to choose  $s = z$ . Then, if the coordinate  $\phi$  takes its values from the interval  $[0, 2\pi)$ , a representation in terms of the non-orthogonal coordinates  $(r, \phi, z)$  is unique and (2.5) yields

$$\nabla V = \frac{\partial V}{\partial r} \mathbf{e}_r + \left( \frac{h}{r} \frac{\partial V}{\partial \phi} + \frac{\varepsilon r}{h} \frac{\partial V}{\partial z} \right) \mathbf{e}_\phi + \frac{\partial V}{\partial z} \mathbf{H}. \quad (3.13)$$

Imposing helical symmetry on the components of  $\mathbf{u} = \nabla V$  requires  $\partial V / \partial z = v_c$ , a constant, so that

$$V(r, \phi, z) = v_c z + v_c U(r, \phi). \quad (3.14)$$

This means that for helical potential flows, the  $\mathbf{H}$ -component of the velocity field must be a constant, namely  $v_c$  (note  $\mathbf{H}$  is not a unit vector.) The other two components for an incompressible fluid are determined by the equation

$$\nabla^2 U = 0, \quad \text{where} \quad \nabla^2 = \frac{1}{r} \frac{\partial}{\partial r} \left( r \frac{\partial}{\partial r} \right) + \frac{h^2}{r^2} \frac{\partial^2}{\partial \phi^2}, \quad (3.15)$$

together with the solid wall boundary condition  $\mathbf{n} \cdot \nabla V = 0$  implying

$$\mathbf{n} \cdot \nabla U = -\frac{\varepsilon r}{h} \mathbf{n} \cdot \mathbf{e}_\phi. \quad (3.16)$$

The same result can be obtained directly from (2.6), (2.7) and (2.8):

$$\boldsymbol{\omega} = 0 \quad \Rightarrow \quad \nabla v = 0, \quad \xi = 0,$$

which leads to

$$v = v_c, \quad \text{a constant, and} \quad \mathcal{L}\Psi = \frac{2\varepsilon}{h^2} v_c, \quad (3.17)$$

where  $\Psi$  is the streamfunction of (2.6), satisfying  $\Psi = 0$  on  $S$ , corresponding to the potential  $V$ . An important consequence of (3.15) and (3.16) or of (3.17) is that even irrotational flows are not uni-directional in helical geometries. It can be shown that

$$\lim_{\varepsilon \rightarrow 0} \mathbf{u} = v \mathbf{e}_z, \quad \lim_{\varepsilon \rightarrow \infty} \mathbf{u} = \frac{v}{r} \mathbf{e}_\theta, \quad (3.18)$$

so that helical flows are structurally more complex than axisymmetric or two-dimensional ones.

## 3.1.1. Exact solution for a rectangular boundary

An explicit formula for the solution can be obtained for a particular shape of the helical pipe. When  $(r, \phi) \in \Omega = [b-a, b+a] \times [0, \phi_0)$ , for some  $\phi_0 < 2\pi$ , then  $S = \partial\Omega$  and  $S_0$  are rectangles (figure 2) and the problem (3.15) with (3.16) takes the form

$$\frac{1}{r} \frac{\partial}{\partial r} \left( r \frac{\partial U}{\partial r} \right) + \frac{h^2}{r^2} \frac{\partial^2 U}{\partial \phi^2} = 0$$

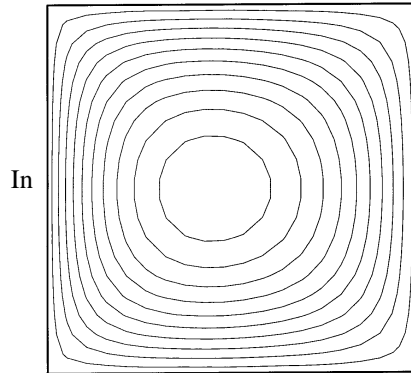


FIGURE 3. Streamlines of the cross-pipe component in potential flow,  $a = 0.5, b = 1.5, \varepsilon = 1$ . 'In' denotes the inside of the helical bend.

with

$$\frac{\partial U}{\partial r} = 0 \quad \text{on} \quad r = b \pm a; \quad \frac{\partial U}{\partial \phi} = -\frac{\varepsilon r^2}{h^2} \quad \text{on} \quad \phi = 0, \phi_0.$$

A solution of the following form can be found:

$$U(r, \phi) = A_0\phi + \sum_{m=1}^{\infty} A_m R_{v_m}(r) \frac{\cosh(v_m(\phi - \frac{1}{2}\phi_0))}{\sinh(\frac{1}{2}v_m\phi_0)}. \tag{3.19}$$

The function  $R_v(r) = I'_{2v}(b-a)I_{1v}(r) - I'_{1v}(b-a)I_{2v}(r)$ , where  $I_{1v}(r), I_{2v}(r)$  are respectively the real and imaginary part of the modified Bessel function  $I_{iv}(i\sqrt{\varepsilon}r)$ . The constants are determined by

$$A_0 = -\frac{\int_{b-a}^{b+a} \varepsilon r \, dr}{\int_{b-a}^{b+a} h^2 r^{-1} \, dr}, \quad \text{and for } m \neq 0, \quad A_m = -\frac{\int_{b-a}^{b+a} R_{v_m}(r) \varepsilon r \, dr}{\int_{b-a}^{b+a} R_{v_m}^2(r) h^2 r^{-1} \, dr}$$

where  $v_m$  can be found numerically as the roots of the equation

$$\begin{vmatrix} I'_{1v}(b-a) & I'_{2v}(b-a) \\ I'_{1v}(b+a) & I'_{2v}(b+a) \end{vmatrix} = 0.$$

For fixed  $\phi_0$  and  $a$ , the flow depends only on the parameters  $\varepsilon$  and  $b$ . The pitch of the helical pipe,  $\varepsilon$ , generates a non-zero torsion which introduces the three-dimensionality, while  $b$  is the radius of the helical pipe centreline and is, rather, responsible for the curvature effects. The curvature  $\kappa$  and torsion  $\tau$  of the pipe centreline can be expressed in terms of  $\varepsilon$  and  $b$ :

$$\kappa = \frac{\varepsilon^2 b}{h_b^2}, \quad \tau = \frac{\varepsilon}{h_b^2}, \quad \text{where } h_b = h_{|r=b} = (1 + \varepsilon^2 b^2)^{1/2}. \tag{3.20}$$

The solution given by (3.19) is valid for arbitrary values of the parameters. However, it appears that the general qualitative characteristics of the flow remain unchanged as  $\varepsilon, b$  vary. Figure 3 portrays a typical contour pattern for the streamfunction  $\Psi$  given by (3.17) corresponding to the velocity potential  $V$  when  $a = 0.5, b = 1.5, \varepsilon = 1$  and  $\phi_0 = 1$ . Since  $\Psi$  is helically symmetric, the closed contours of  $\Psi$  define a family of helical tubes which are streamsurfaces of the flow. At the point where  $\Psi$  is maximum

the cross-pipe motion has a stagnation point, and the helical tube reduces to a centre streamline carrying a fluid particle in the  $\mathbf{H}$ -direction with velocity  $v/h$ . The other streamlines follow their paths on the helical streamsurfaces, so that a fluid particle travels down the pipe with the flow,  $v\mathbf{H}$ , as well as going around the centre-streamline with the velocity determined by  $\Psi$ .

For relatively large  $\varepsilon$ , the centre-streamline lies closer to the left and the greatest cross-pipe velocity occurs in the region near the inner wall, to the left of the centre-streamline. As  $\varepsilon$  is decreased to a very small value the centre streamline moves slightly to the right and the velocity is greatest near the outer wall, on the right of the centre streamline. As  $\varepsilon$  approaches its limits,  $\varepsilon \rightarrow 0, \infty$ , the motion becomes unidirectional (3.18). The cross-pipe potential flow component is thus a result of torsion.

### 3.2. Inertially dominated steady flows

As is usual for internal flows at high Reynolds number, the driving force must be balanced by viscous forces in some average sense, while at leading order inertia determines the shape of the flow. If  $\Psi$ ,  $v$  and  $\xi$  are rescaled with  $R$ , the governing equations can be written in the form

$$h^{-2}\mathbf{H} \cdot (\nabla\Psi \times \nabla v) = R^{-1} \left( 1 + \mathcal{L}v + \frac{2\varepsilon}{h^2}\xi \right), \quad (3.21)$$

$$h^{-2}(\xi\nabla\Psi + v\nabla v) = \nabla(p + \frac{1}{2}|\mathbf{u}|^2) - R^{-1}\mathbf{H} \times \nabla\xi, \quad (3.22)$$

where the vorticity equation has been replaced by the two momentum equations and  $p = p(r, \phi)$  is the (rescaled) pressure. If a streamline does not pass through a boundary layer then the (rescaled) velocity will be  $O(1)$  as  $R \rightarrow \infty$ , but if every streamline passes through a high-shear region, as in §4.1.2 below, different scalings apply. In either case, away from such regions, to leading order,

$$\mathbf{H} \cdot (\nabla\Psi \times \nabla v) = 0 \Rightarrow v = v(\Psi). \quad (3.23)$$

Now if  $B = p + \frac{1}{2}|\mathbf{u}|^2$  denotes the total Bernoulli pressure, equation (3.22) without the viscous term requires  $B = B(\Psi)$  in order to ensure that  $\nabla B$  is parallel to  $\nabla\Psi$ . Then (3.22) yields

$$\xi + v'v = h^2 B'. \quad (3.24)$$

From (2.8) it then follows that the cross-pipe flow is determined by

$$\mathcal{L}\Psi = \frac{2\varepsilon}{h^2}v - vv' + h^2 B' \quad (3.25)$$

with

$$\Psi = 0 \quad \text{on } S,$$

where  $v = v(\Psi)$  and  $B = B(\Psi)$  are two unknown functions.

Another possible solution to (3.21) and (3.22) for large  $R$  is the ‘unidirectional’ (but rotational) flow  $\Psi = 0$ ,  $\mathbf{u} = v(r)\mathbf{H}$  where  $v(r)$  is an arbitrary function. (Note from (2.1) that the direction  $\mathbf{H}$  varies with both  $r$  and  $\theta$ .) Such an asymptotic state is considered in §4.1.2.

Helically symmetric flows may be regarded as having closed streamlines and hence arguments akin to those of the Prandtl–Batchelor results Batchelor 1956 can be used for genuinely steady flows to fix the unknown functions  $v(\Psi)$  and  $B(\Psi)$ . In helical geometry these functions are determined by a system of integro-differential equations Childress *et al.* 1989, and are not particularly simple. However, the Prandtl–Batchelor arguments rely on the small viscous forces having sufficient time to act in a fully

developed flow. In practice this would require a very long helical pipe length and for particular applications, it may be more relevant to consider other functions  $B(\Psi)$ ,  $v(\Psi)$ . An inviscid entry problem could have an arbitrary upstream vorticity and Bernoulli head, for example.

A particular solution can be found if we choose  $B'$  and  $v$  to linearize (3.25). If  $B' = 0$  and  $v(\Psi) = v^0 + \lambda\Psi$ , then writing  $\Psi = v^0\Psi^*$  the flow is determined (compare Dritschel 1991) by

$$\begin{aligned} \mathcal{L}\Psi^* + \left(\lambda^2 - \frac{2\varepsilon}{h^2}\lambda\right)\Psi^* &= \frac{2\varepsilon}{h^2} - \lambda, \\ \Psi^* &= 0 \quad \text{on } S. \end{aligned} \tag{3.26}$$

Note that the flow given by (3.26) is rotational. From (3.24) it follows that

$$\boldsymbol{\omega} = -v'\mathbf{u} + h^2B'\mathbf{H}$$

and for  $B' = 0$  this means that  $\boldsymbol{\omega}$  is parallel to  $\mathbf{u}$ , so that (3.26) defines a Beltrami flow.

An explicit formula for the solution of (3.26) can be obtained in the case when the contour  $S$  is rectangular in a manner similar to (3.19). One can verify that a particular integral for (3.26), for all  $\lambda \neq 0$ , is the function

$$\Psi_c^*(r) = -\frac{1}{\lambda} + C_1(J_0(\lambda r) + \varepsilon r J_1(\lambda r)) + C_2(Y_0(\lambda r) + \varepsilon r Y_1(\lambda r)),$$

where  $J_\nu, Y_\nu$  denote the Bessel functions of respectively the first and second kind, while the constants  $C_1, C_2$  are determined by  $\Psi_c^*(b \pm a) = 0$ . The solution of (3.26) thus takes the form

$$\Psi^*(r, \phi) = \Psi_c^*(r) + \sum_{m=1}^{\infty} A_m R_{v_m}(r) \frac{\cosh(v_m(\phi - \frac{1}{2}\phi_0))}{\cosh(\frac{1}{2}v_m\phi_0)}. \tag{3.27}$$

The function  $R_{v_m}(r) = J_{2v_m}(b-a)J_{1v_m}(r) - J_{1v_m}(b-a)J_{2v_m}(r)$  where  $J_{1v_m}(r), J_{2v_m}(r)$  are respectively the real and imaginary part of  $J_{iv_m}(\mu r) - \varepsilon r \mu / \lambda J'_{iv_m}(\mu r)$  with  $\mu^2 = \lambda^2 + v^2\varepsilon^2$ . The constants are given by

$$A_m = -\frac{\int_{b-a}^{b+a} R_{v_m}(r)\Psi_c^*(r)r^{-1}dr}{\int_{b-a}^{b+a} R_{v_m}(r)r^{-1}dr}$$

and the eigenvalues  $v_m$  satisfy  $\begin{vmatrix} J_{1v_m}(b-a) & J_{2v_m}(b-a) \\ J_{1v_m}(b+a) & J_{2v_m}(b+a) \end{vmatrix} = 0$ , which can be solved numerically.

The solution given by (3.27) resembles the irrotational flow (3.19) and can be obtained for arbitrary values of the parameters  $\varepsilon$  and  $a/b$ . A typical cross-pipe flow is drawn in figure 4. Qualitatively the streamlines appear similar to those of figure 3 but there are important differences. The  $\mathbf{H}$ -component of the velocity is no longer constant and depends on the values of  $\Psi^*$ . This means that different helical streamsurfaces travel down the pipe with different velocities which generates vorticity. This vorticity obeys the Beltrami condition so that the streamlines and vortex lines follow the same trajectories in space. The centre-streamline of this rotational flow is shifted to the right, closer to the outer wall, compared to the potential flow. The cross-pipe wall shear component on the outer bend might therefore be expected to be larger for rotational flows.

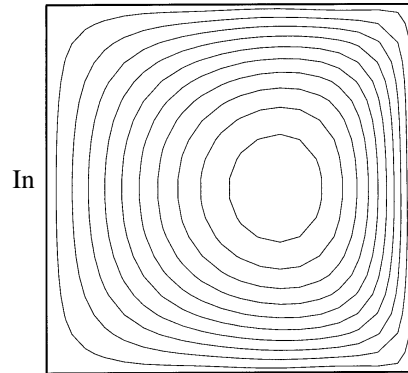


FIGURE 4. Streamlines of the rotational cross-pipe flow for  $\varepsilon = 1$ ,  $\lambda = 1$ ,  $a = 0.5$ ,  $b = 1.5$ . The maximum of  $\Psi$  is towards the outside of the bend compared to the potential flow of figure 3.

#### 4. The numerical approach

Although helical symmetry essentially reduces the problem to two dimensions, the equations remain nonlinear and analytical progress is rather limited. Thus finite difference schemes have been developed for solving the time-dependent, helically symmetric Navier–Stokes equations driven by an imposed down-pipe pressure. In this paper a steady pressure gradient is assumed, while time-periodic forcing is discussed in ZM2. The written code nevertheless follows the time-evolution of an initial flow and allows for two types of pipe geometry: rectangular and circular.

##### 4.1. Rectangular pipe

If the pipe cross-section is taken to be the rectangle  $0 \leq \phi \leq \phi_0$ ,  $b-a \leq r \leq b+a$ , then the boundary consists of  $(r, \phi)$  coordinate surfaces. In this case it is particularly easy to impose the boundary conditions and a finite difference scheme can be implemented using a regular grid in  $(r, \phi)$  variables.

An explicit method, second order in space and first order in time, is used to solve the equations (3.9) and (3.10). A Gauss–Seidel routine is applied to the elliptic problem (3.11), using a block method Strikwerda 1989. Initially, the fluid is assumed to be at rest,  $\Psi, v = 0$ , and motion is generated when the pressure gradient (3.1) is applied. Then the time evolution is controlled by the equations (3.9) and (3.10) which, for a given  $\Psi^j, v^j, \xi^j$  at time  $t = j\delta t$ , determine  $v^{j+1}, \xi^{j+1}$  at the time level  $t + \delta t$  in the interior of the flow. These new values are substituted into the right-hand side of (3.11) which, with  $\Psi = 0$  on  $S$ , is solved to find  $\Psi^{j+1}$ . The no-slip condition  $\partial\Psi/\partial n = 0$  on the wall is used to define  $\xi^{j+1}$  on the boundary. The computation is continued until the flow has reached a fully developed (steady) state. A similar implicit scheme, based on a three-time-level algorithm (Fletcher 1991), was also developed. This was more efficient computationally, and essential for the time-periodic problems considered in ZM2.

##### 4.1.1. Numerical accuracy

The finite difference codes use centred spatial differences, so that if all the flow structures are properly resolved, numerical errors in the steady state should be of second order in the mesh length. A standard test can be performed in order to ensure that such an accuracy is indeed achieved.

As an example, consider the flow inside a rectangular helical pipe driven by a steady pressure gradient when  $R = 30^3 h_b$ ,  $b = 1.5$ ,  $a = 0.5$ ,  $\varepsilon = 1$  and  $\phi_0 = 1$ . For large  $N$ , one assumes that  $\Psi \sim \Psi_N + A(1/N)^\gamma$  (and similarly  $v, \xi$ ), where  $\Psi, v, \xi$  represent the

$N \times N$	$10^4 \Psi_{max}$	$10^2 v_{max}$	$10 \xi_{max}$	$10^4 \tilde{\Psi}$	$10^2 \tilde{v}$	$10 \tilde{\xi}$
$60 \times 60$	6.07443	3.1856	2.4520	5.19707	2.3779	-0.54093
$80 \times 80$	6.07074	3.1862	2.4409	5.19416	2.3803	-0.54035
$160 \times 160$	6.06731	3.1868	2.4300	5.19144	2.3825	-0.53981
$\gamma$	2.09	1.80	1.96	2.076	2.062	2.069

TABLE 1. Numerical accuracy check ( $\gamma \simeq 2$ ) for  $R = 30^3 h_b$ ,  $a = 0.5$ ,  $b = 1.5$ ,  $\varepsilon = 1$ .

exact solution and  $\Psi_N, v_N, \xi_N$  a solution obtained on an  $N \times N$  grid. As  $N$  varies, data from three different grids determine  $\gamma$  uniquely. Table 1 presents a computation of  $\gamma$  based firstly on the maximum norm over the whole grid ( $\Psi_{max}$  etc.) and secondly at the particular point  $r = 1.5$ ,  $\phi = 0.5$ , writing  $\tilde{\Psi} = \Psi(1.5, 0.5)$  etc.

In all cases  $\gamma$  is close to 2, indicating the desired second-order convergence to the exact solution. The maximum norm for  $v_{max}$  is the least reliable as the point at which it applies varies over the grid, especially given the degeneracy of  $v_{max}$  evident from figure 5. From the table it is also possible to estimate the constant  $A$  which is never bigger than 10.

The smaller grid  $40 \times 40$  was also considered for this case and although the computed solution appeared qualitatively plausible, the numerical values lead to  $\gamma \sim 1$  (using  $N = 40, 60, 80$ ), suggesting inadequate resolution for  $N = 40$ , especially inside the boundary layers. It is often a good idea to use non-uniform grids for flows with a boundary layer structure. However, should these layers separate into the interior (see figure 10 in ZM2) it can be important to have uniform resolution. The required number of points is consistent with  $N \sim R^{1/3}$ , as suggested by the discussion below. Similar tests have been performed for other helical flows discussed in the present work and ZM2.

#### 4.1.2. Solution for large $R$

With the steady pressure gradient (3.1), on physical grounds one expects a steady state to be approached as  $t \rightarrow \infty$ , and the numerical simulations confirm this. The problem of uniqueness, long-time behaviour and regularity of helical solutions to the Navier–Stokes equations is discussed in Mahalov, Titi & Leibovich (1990) for the case of Hagen–Poiseuille flow.

It can easily be derived from (3.9), (3.10) that such a steady flow must satisfy the equations

$$\left. \begin{aligned} \frac{1}{r} J(\Psi, v) &= R + \mathcal{L}v + \frac{2\varepsilon}{h^2} \xi, \\ \frac{1}{r} J(\Psi, \xi) + \frac{2\varepsilon^2}{h^2} \left( \xi \frac{\partial \Psi}{\partial \phi} + v \frac{\partial v}{\partial \phi} \right) &= \frac{2\varepsilon}{h^2} R + \mathcal{L}\xi, \\ \mathcal{L}\Psi &= \frac{2\varepsilon}{h^2} v + \xi. \end{aligned} \right\} \quad (4.1)$$

If the geometry of the helical boundary is defined, so that the rectangular contour  $S$  and  $\varepsilon$  are determined, the flow governed by (4.1) is controlled only by the parameter  $R$ . Computations have been carried out for different values of  $R$ , which plays a rôle similar to the Reynolds or Dean number. In the case of  $S : 1 \leq r \leq 2, 0 \leq \phi \leq 1$  ( $a = 0.5, b = 1.5$ ) and  $\varepsilon = 1$ , solutions have been obtained for  $R$  between 1 and  $64\,000 h_b$ . Defining a rectangular Dean number  $D = R/h_b(a/b)$ , the highest value considered corresponds roughly to  $D = 21\,000$ . However, as the curvature decreases to say  $a/b = 0.1$ , which is more appropriate for the Dean approximation, the same

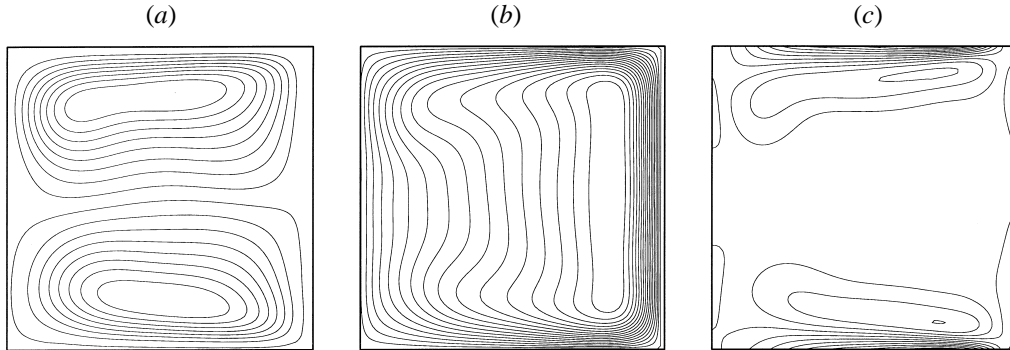


FIGURE 5. Flow for  $\varepsilon = 1$ ,  $a = 0.5$ ,  $b = 1.5$ ,  $\phi_0 = 1$  and  $R = 40^3 h_b$ . (a)  $\Psi$ , (b)  $v$ , (c)  $\xi$ . At high  $R$ , the flow is nearly top-down symmetric and in the core  $v \simeq v(r)$  increasing towards the outside of the bend.

value of  $R$  gives a Dean number around 6400. Since the flow patterns for both small and intermediate values of  $R$  are qualitatively similar to the corresponding ones in circular geometry, these will be discussed later and here only the case of large  $R$  will be addressed.

Figure 5 portrays contours in the  $(r, \phi)$ -plane of respectively, left to right,  $\Psi$ ,  $v$ ,  $\xi$  at  $R = 64000 h_b$ . In this case the cross-pipe motion consists of two vortices, i.e. two recirculating regions, which become symmetric as  $R \rightarrow \infty$ . The streamlines appear to pass through a thin wall region. The down-pipe velocity  $v$  has very little  $\phi$ -variation away from the boundaries while the vorticity  $\xi$  is nearly constant in the interior and is mostly accumulated in thin wall regions at the top and bottom. There is some suggestion of an intermediate layer between the core and the horizontal wall layers. All of this suggests that an asymptotic structure emerges as  $R \rightarrow \infty$ . Standard boundary layer arguments predict appropriate scalings which agree with these observations.

In the governing equation, a balance between pressure gradient and inertia in the core and between inertia and viscous forces in the  $\phi$  boundary layers (top and bottom) gives  $\Psi \sim \delta^{-1}$ ,  $v \sim R\delta$ , where  $\delta$  is the thickness of the layer. The scale of the vorticity  $\xi$  can be determined from the kinematic relation (2.8). In the core  $\xi = \xi_c \sim v$ , since the primary (down-pipe) flow is dominant, while in the boundary layer  $\xi \sim \Psi \delta^{-2}$ . For the cross-pipe motion to be centrifugally driven, then the quadratic term in the vorticity equation must be of the same order as the viscous term,  $v^2 \delta^{-1} \sim \xi \delta^{-2}$ . This yields  $\delta = R^{-1/3}$  and  $\Psi \sim R^{1/3}$ ,  $v \sim R^{2/3}$ ,  $\xi_c \sim R^{2/3}$ ,  $\xi \sim R$ . Hence, the equation (4.1) at leading order in the core takes the form

$$\begin{aligned} \frac{1}{r} J(\Psi, v) &= R, \\ \frac{2\varepsilon^2}{h^2} v \frac{\partial v}{\partial \phi} &= 0, \\ \frac{2\varepsilon}{h^2} v + \xi_c &= 0, \end{aligned}$$

which leads to

$$\Psi = R^{1/3} \frac{r}{c'(r)} \phi, \quad v = R^{2/3} c(r), \quad \xi_c = -R^{2/3} \frac{2\varepsilon}{h^2} c(r), \quad (4.2)$$

for an unknown function  $c(r)$ . If  $\xi_c$  is genuinely constant, this would suggest  $c(r) \propto h^2 = 1 + \varepsilon^2 r^2$  and the cross-pipe flow would have no  $\phi$ -component.



In the boundary layers at the top and bottom the scalings imply

$$\left. \begin{aligned} \frac{1}{r} J(\Psi, v) &= \frac{h^2}{r^2} \frac{\partial^2 v}{\partial \phi^2}, \\ \frac{1}{r} J(\Psi, \xi) + \frac{2\varepsilon^2}{h^2} \left( \xi \frac{\partial \Psi}{\partial \phi} + v \frac{\partial v}{\partial \phi} \right) &= \frac{h^2}{r^2} \frac{\partial^2 \xi}{\partial \phi^2}, \\ \frac{h^2}{r^2} \frac{\partial^2 \Psi}{\partial \phi^2} &= \xi. \end{aligned} \right\} \quad (4.3)$$

As  $\varepsilon, b \rightarrow \infty$ , equation (4.1) yields the Dean equations for an axisymmetric pipe. The problem of large Dean number asymptotics has attracted much attention, yet a complete solution is still not known. In rectangular geometry an asymptotic structure was proposed by Smith (1976). The above scaling relies on essentially the same ideas and gives the same equations in the Dean limit. It is not difficult to write down equations for the boundary layer at the outer wall of the bend, where  $r$  is constant. There, as  $h = h(r)$ , the equations are identical with those of axisymmetry. However, the main difficulty is caused by the fluid behaviour at the inner wall where the flow leaves the boundary layer and enters the core. An entirely similar structure arises in pipes with a circular cross-section. In the Dean problem a global description has not yet been found (Dennis & Riley 1991). The core flow solution (4.2) is known only when the function  $c(r)$  is determined which cannot be done independently of solving the boundary layer equation (4.3). The fact that the governing equations (4.1) include geometrical terms which vanish as  $\varepsilon \rightarrow \infty$  and are not present in the axisymmetric equation raised hope that this could render the helical case simpler in the limit  $R \rightarrow \infty$ . But, as follows from (4.2) and (4.3), these extra terms do not appear at leading order at the inner wall, so that a similar difficulty is faced in the helical case as in the Dean problem.

#### 4.2. Circular pipe

From (2.12), the Jacobian  $J = 0$  when  $\rho = 0$  and the transformation  $\mathcal{T}$  is singular on the centreline of the pipe. Therefore, the point  $\rho = 0$  requires special treatment in the numerical method. Since the fluid mechanical equations derive from physical conservation laws it is possible to transform them into divergence form. In the helical case one obtains

$$\frac{\partial v}{\partial t} + \nabla \cdot (v\mathbf{u}) = R + \mathcal{L}v + \frac{2\varepsilon}{h^2} \xi, \quad (4.4)$$

$$\frac{\partial \xi}{\partial t} + h^2 \nabla \cdot \left( \frac{\xi}{h^2} \mathbf{u} - \frac{v}{h^2} \boldsymbol{\omega} \right) = \mathcal{L}\xi - \frac{2\varepsilon}{h^2} \left( \mathcal{L}v + \frac{2\varepsilon}{h^2} \xi \right), \quad (4.5)$$

where the operator  $\mathcal{L}$  may be written as  $\mathcal{L} = h^2 \nabla \cdot (h^{-2} \nabla)$ . In order to determine the time evolution at the coordinate singularity  $\rho = 0$  it is necessary to evaluate there all the spatial derivatives which appear in (4.4) (4.5). It can be shown that integrating over the small volume element  $\rho \leq a_0$  ( $a_0$  can be half of the mesh size) and applying Green's theorem yields

$$\mathcal{L}f|_{\rho=0} = \left( \frac{a_0}{2} \int_0^{2\pi} \left( \frac{rJ}{h^2} \right)_{|\rho=a_0} d\eta \right)^{-1} \int_0^{2\pi} \left( \frac{rJ}{h^2} \frac{\partial f}{\partial \rho} \right)_{|\rho=a_0} d\eta + O(a_0^2),$$

$$\nabla \cdot (v\mathbf{u})|_{\rho=0} = \left( \frac{a_0}{2} \int_0^{2\pi} rJ|_{\rho=a_0} d\eta \right)^{-1} \int_0^{2\pi} \left( v \frac{\partial \Psi}{\partial \eta} \right)_{|\rho=a_0} d\eta + O(a_0^2),$$

$b$	2	5	10	20	30	100	200	$\infty$
$D = 500, \varepsilon = 100$								
$\gamma_s/\gamma_c$	—	1.3995	1.3719	1.3570	1.3517	—	—	1.337
$v_{max}$	—	74.523	78.677	80.995	81.791	—	—	83.7
$\Psi_{max}$	—	5.701	5.925	6.039	6.077	—	—	6.12
$D = 5000, \varepsilon = 1000$								
$\gamma_s/\gamma_c$	2.6903	—	—	2.480	—	2.4569	2.4539	2.392
$v_{max}$	325.53	—	—	427.65	—	440.93	442.64	449.3
$\Psi_{max}$	16.18	—	—	20.10	—	20.48	20.53	19.97

TABLE 2. Comparison of results with the Dean limit  $\varepsilon, b \rightarrow \infty$  as given by Collins & Dennis (1975).

$$h_b^2 \nabla \cdot \left( \frac{\xi}{h^2} \mathbf{u} - \frac{v}{h^2} \boldsymbol{\omega} \right) \Big|_{\rho=0} = \left( \frac{a_0}{2} \int_0^{2\pi} \left( \frac{rJ}{h^2} \right) \Big|_{\rho=a_0} d\eta \right)^{-1} \int_0^{2\pi} \left( \frac{\xi}{h^2} \frac{\partial \Psi}{\partial \eta} + \frac{v}{h^2} \frac{\partial v}{\partial \eta} \right) \Big|_{\rho=a_0} d\eta + O(a_0^2).$$

The above formulae can easily be discretized and substituted into the numerical equations to eliminate the effect of the coordinate singularity. When a finite difference scheme is written in term of  $(\rho, \eta)$  variables the same algorithms as for the rectangle can be used to compute steady helical flows in a circular pipe.

4.2.1. *Results and discussion*

Steady motion in a curved, circular pipe appears in many practical applications and has attracted much numerical study. The present analysis allows for a pipe with arbitrary (constant) curvature and torsion controlled respectively by the parameters  $b$  and  $\varepsilon$  as in (3.20). As these parameters tend to infinity the Dean equations can be recovered for which a considerable amount of numerical data has been published, for example Collins & Dennis (1975). The present numerical results may be compared both for validation purposes and to quantify the effects of finite  $b$  and  $\varepsilon$ . Table 2 lists the maximal primary flow velocity  $v_{max}$ , the maximum of the streamfunction  $\Psi_{max}$  and the pipe resistance

$$\frac{\gamma_s}{\gamma_c} = \frac{\pi R}{8} h_b \int_0^1 \int_0^{2\pi} v \frac{rJ}{h^2} d\rho d\eta$$

obtained for different  $b$  as  $\varepsilon \rightarrow \infty$ . All the numbers have been rescaled as  $v \sim Dh_b$ ,  $\Psi \sim R/h_b$  in order to allow for comparison with the last column  $b = \infty$ , corresponding to the Dean problem and containing data from Collins & Dennis (1975). As expected, as the radius  $b$  becomes large the pipe resistance  $\gamma_s/\gamma_c$  decreases and the velocity  $v_{max}$  increases so that in the limit of small curvature and large  $\varepsilon$  the values resulting from the Dean equations are approached. The relatively large values  $b = 100, 200$  in the case of  $D = 5000$  (the highest given by Collins & Dennis) suggest that the curvature effects, neglected in the Dean limit, are more significant at higher Dean number. In general, as  $\varepsilon, b \rightarrow \infty$  the numerical solution is in reasonable agreement with previous studies, with the greatest discrepancies, as one would expect, occurring at high Reynolds numbers.

The flow behaviour for  $O(1)$  curvature and torsion and various values of  $R$  has been investigated. For the helical pipe  $a = 1, b = 2$  and  $\varepsilon = 1$  the numerical solution in the range  $R = 1-50^3$  has been obtained and three flow patterns plotted in the  $\mathbf{H}_b$ -plane, corresponding to  $R = 1, 160, 3375$ , are shown in figure 6. Interestingly,

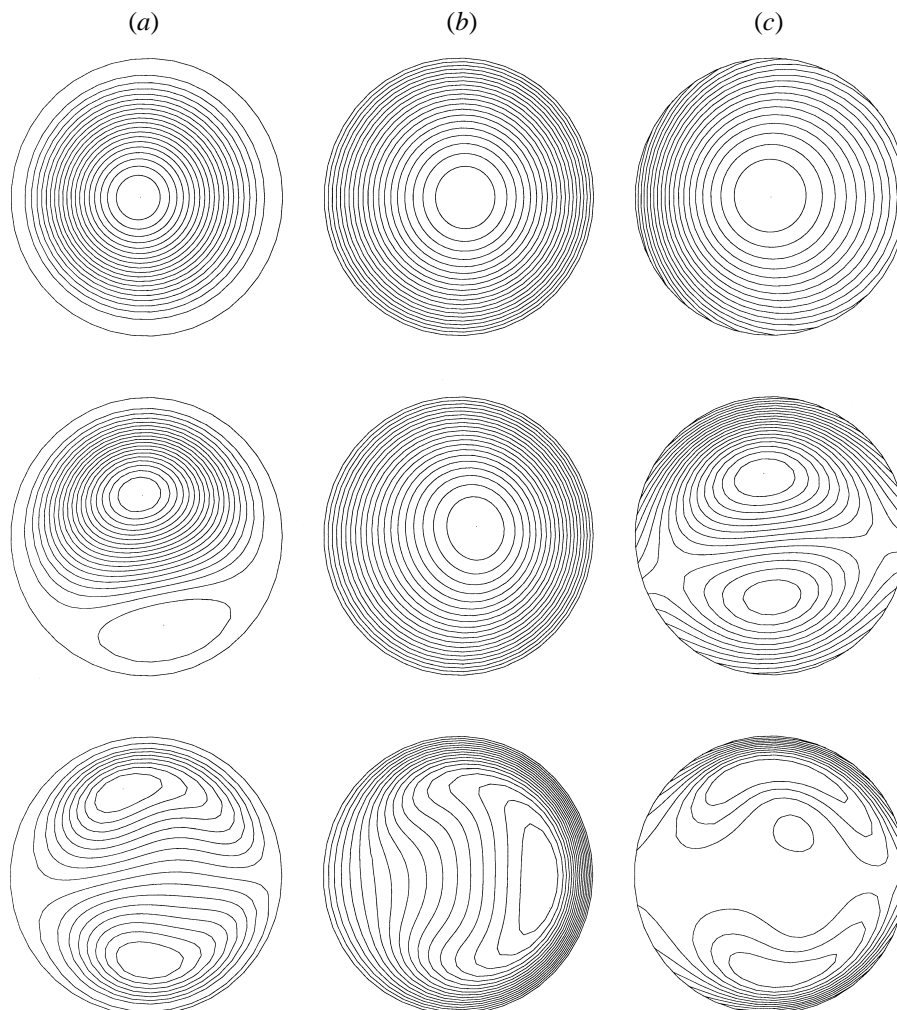


FIGURE 6. Flow ((a)  $\Psi$ , (b)  $v$ , (c)  $\xi$ ) for  $a = 1$ ,  $b = 2$ ,  $\varepsilon = 1$ . Top:  $R = 1$ , middle:  $R = 160$ , bottom:  $R = 3375$ . As  $R$  increases the cross-pipe flow ( $\Psi$ ) changes from one-vortex to symmetrical two-vortex type.

differing qualitative behaviour can be observed as  $R$  varies. When  $R$  is small, the cross-pipe motion has one-vortex structure and the down-pipe velocity profile is nearly quadratic in  $r$ . As  $R$  is increased ( $R > 100$ ) another circulating region at the bottom of the pipe is formed. This second vortex, which is initially small, develops and grows while at the same time the maximum of the velocity  $v$  is pushed towards the outer bend. Hence, for intermediate and large  $R$  the secondary motion consists of two recirculating regions and the flow becomes almost symmetric. For  $R = 3375$ , the asymptotic state has not been reached, although some hint of it can be discerned.

This type of transition between one- and two-vortex solutions and the change from asymmetric to symmetric flow structure is not observed in axisymmetry and is an effect of torsion. A stagnation point (or helical stagnation line) of the secondary flow is associated with low cross-pipe shear. This is possibly relevant to the fact that atherosclerotic lesions sometimes adopt helical patterns (Masawa, Glagov & Zarins 1994).

Some aspects of the mechanism which is responsible for such behaviour can be deduced from the limit  $R \rightarrow 0$ , corresponding to a small Dean number analysis (Dean 1928). Expanding  $\Psi \sim \Psi_0 + R\Psi_1 + \dots$  and so on, at leading order the flow is governed by the Stokes equations with a constant pressure gradient,

$$\left. \begin{aligned} \mathcal{L}v + \frac{2\varepsilon}{h^2}\xi + 1 &= 0, \\ \mathcal{L}\xi + \frac{2\varepsilon}{h^2} &= 0, \\ \mathcal{L}\Psi &= \frac{2\varepsilon}{h^2}v + \xi. \end{aligned} \right\} \quad (4.6)$$

In axisymmetry ( $\varepsilon \rightarrow \infty$ ), equation (4.6) defines a unidirectional flow but for finite  $\varepsilon$  a cross-pipe motion is generated at leading order. Numerical calculation shows that only one circulating region develops. At next order in  $R$ , just as found by Dean (1928) in axisymmetry, a cross-flow emerges with a two-vortex pattern. Such a two-vortex solution is of  $O(R)$  while the leading-order term is proportional to  $(\varepsilon/h_b^2)$ . Thus, for every  $0 < \varepsilon < \infty$ , at very low Reynolds number the one-vortex pattern is dominant, as is observed numerically. As  $R$  is increased the second-order effects become more important and above a certain critical value the second circulating region can be seen. For large  $\varepsilon$  this critical value lies within the regime of small- $R$  asymptotics and then the transition between the two structures appears as a linear superposition of the first- and second-order solutions. When  $\varepsilon$  is arbitrary the situation is more complex and is controlled by nonlinear interaction, but the change from one- to two-vortex solutions is plausible.

Computations have been carried out to discover the effect of varying  $\varepsilon$  for  $R = 125$  and  $R = 1000$  and behaviour similar to that discussed above has been found. When  $\varepsilon$  is decreased the solution becomes asymmetric and eventually the second vortex at the bottom of the pipe completely disappears. In the case  $R = 1000$ , boundary layers (thicker than those in the axisymmetric case) are formed. In the limit  $\varepsilon \rightarrow 0$ , however, all the steep gradients decrease and the vorticity accumulated at the bottom of the pipe diffuses away from the wall. At the same time the maximum of  $v$  moves first slightly to the top and then towards the centre of the pipe (figure 7). To a certain extent, the observed flow patterns can be understood physically. A helical flow can be regarded as motion in the  $z$ -direction and rotation around the  $z$ -axis. Large values of  $R$  generate a strong centrifugal force which makes the fluid feel mostly the rotation effect. In such a case the quadratic term  $vv_\phi$  determines the vorticity distribution. In contrast, smaller values of  $\varepsilon$  yield a straighter pipe which favours motion in the  $z$ -direction. Then, the geometrical term  $2\varepsilon/h^2R$  in the vorticity equation becomes more significant and may even dominate the centrifugal effect.

Figure 8 portrays the flow at the very large  $R = 50^3$ . In this case, as discussed in §4.1.2, an asymptotic structure with inviscid core and viscous boundary layers emerges. The core flow is almost uni-directional, varying only with  $r$ , while approximate top-down symmetry is discernible. The boundary layers on the top and bottom break down near the inside of the bend, and the flow separates into the core. This separation seems to occur earlier than is observed in the Dean problem, so that  $O(1)$  curvature and torsion may retain some influence on the flow structure even as  $R \rightarrow \infty$ . Letting  $\varepsilon \rightarrow \infty$  with  $a/b$  fixed results in a very similar flow structure to figure 8. It is only as  $b \rightarrow \infty$  also that Dean flow is approached.

A notable feature of the solution in figure 8 is that near the separation points on the inner wall, closed contours of  $v$  and  $\Psi$  appear. Furthermore, these contours suggest a functional relation  $v = v(\Psi)$  of the form (3.23). This implies an inviscid

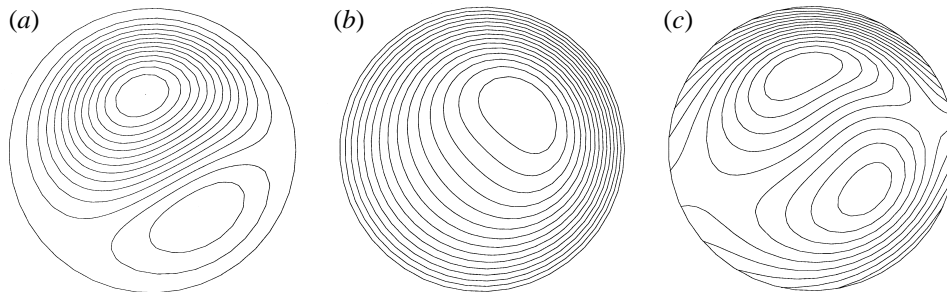


FIGURE 7. Flow in a stretched, almost two-dimensional helical pipe.  $a = 1$ ,  $b = 2$ ,  $\varepsilon = 0.1$  for  $R = 1000$ . (a)  $\Psi$ ; (b)  $v$ ; (c)  $\xi$ . The inside of the bend is on the left.

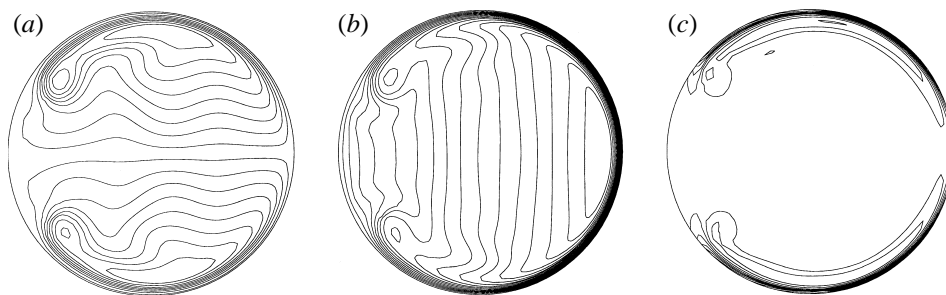


FIGURE 8. Flow ((a)  $\Psi$ , (b)  $v$ , (c)  $\xi$ ) at very large  $R = 50^3$  ( $a = 1$ ,  $b = 2$ ,  $\varepsilon = 1$ ). An asymptotic structure is emerging with  $R^{-1/3}$  boundary layers which separate before the inside of the bend.

structure to the post-separation region, and may provide a clue to the asymptotics. In this inertia-dominated region, the viscous forces would balance the forcing only in some average integral sense along Prandtl–Batchelor lines (Childress *et al.* 1989).

#### 4.3. Multiple solutions

At moderately high Dean number, the axisymmetric, low-curvature Dean problem is known to possess multiple solutions. Dennis & Ng (1982) reported a bifurcation of the Dean two-vortex cross-pipe flow to one with a four-vortex pattern. Daskopoulos & Lenhoff (1989) found further four-vortex solutions, although they argued that only one of these was stable. Even this state has been claimed to be unstable when top-bottom symmetry is not imposed, implying that only the two-vortex solution should be observed in practice (Yanase *et al.* 1989). Nevertheless, for axisymmetric flows with high curvature, so that the Dean equations are inappropriate, Cheng & Mok (1986) report the appearance of a four-vortex solution experimentally. We have not found such a solution numerically.

In the present work, multiple solutions have not been observed for steady helical flows, yet neither have they been exhaustively sought. For no parameter values were two different steady solutions found, although for time-periodic flows, as discussed in ZM2, a symmetry-breaking bifurcation was indeed discovered. It should be remembered that the time-evolution numerical method would not locate solutions which are unstable to helically symmetric disturbances. Also, top-down symmetry is not imposed in the current work, permitting a wider class of instability to manifest itself. The authors suspect that there are no stable, steady four-vortex solutions in helical symmetry, even for nearly axisymmetric flows, but this has not been conclusively shown.

The authors would like to acknowledge with gratitude various helpful discussions with C. G. Caro and J. T. Stuart. Dr Zabielski was supported partly by grants from the Jan Dzienisiewicz Trust, the *Tempus* programme and the Harry Jones fund.

### Appendix. The operator $\mathcal{L}$ in circular geometry

The helical Laplacian in general coordinates, say  $(\rho, \eta)$ , can be expressed in the following way:

$$\begin{aligned} \mathcal{L} = & |\nabla\rho|^2 \frac{\partial^2}{\partial\rho^2} + 2\nabla\rho \cdot \nabla\eta \frac{\partial^2}{\partial\rho\partial\eta} + |\nabla\eta|^2 \frac{\partial^2}{\partial\eta^2} \\ & + \left( \frac{\partial^2\rho}{\partial r^2} + \frac{h^2}{r^2} \frac{\partial^2\rho}{\partial\phi^2} \right) \frac{\partial}{\partial\rho} + \left( \frac{\partial^2\eta}{\partial r^2} + \frac{h^2}{r^2} \frac{\partial^2\eta}{\partial\phi^2} \right) \frac{\partial}{\partial\eta} \\ & + \frac{1 - \varepsilon^2 r^2}{rh^2} \left( \frac{\partial\rho}{\partial r} \frac{\partial}{\partial r} + \frac{\partial\rho}{\partial r} \frac{\partial}{\partial\eta} \right). \end{aligned} \quad (\text{A } 1)$$

In the case of the transformation (2.9)

$$|\nabla\rho| = 1, \quad \nabla\rho \cdot \nabla\eta = 0, \quad |\nabla\eta| = \frac{h}{rJ},$$

where  $J$  is given by (2.12). All the first derivatives which appear in (A 1) can be substituted from (2.11) while the elements of the Hessian take the following form:

$$\begin{aligned} \frac{\partial^2\rho}{\partial r^2} &= \frac{\rho}{h_b^4 r^4 J^2} \left( 2\rho^2 + b^2 h^4 + 3\rho b h^2 \cos\eta - 2\rho h_b r J \right. \\ &\quad \left. - 2b h_b r \cos\eta J - \rho h_b r^2 \frac{\partial J}{\partial r} - b h^2 h_b r^2 \cos\eta \frac{\partial J}{\partial r} \right), \\ \frac{\partial^2\rho}{\partial\phi^2} &= \frac{\rho}{2h_b^4 r^2 J^2} \left( \rho^2 - 2\rho^2 h_b^2 + \rho^2 h_b^4 + 2b^2 h_b^4 - 2\rho b h_b^2 \cos\eta \right. \\ &\quad \left. + 4\rho b h_b^4 \cos\eta - \rho^2 \cos(2\eta) + \rho^2 h_b^4 \cos(2\eta) - 2b h_b^4 r \sin\eta \frac{\partial J}{\partial\phi} \right. \\ &\quad \left. + \rho h_b^2 r \sin(2\eta) \frac{\partial J}{\partial\phi} - \rho h_b^4 r \sin(2\eta) \frac{\partial J}{\partial\phi} \right), \\ \frac{\partial^2\eta}{\partial r^2} &= \frac{b \sin\eta}{h_b^2 r^4 J^2} \left( b h^4 \cos\eta + 2h_b r J + h^2 h_b r^2 \frac{\partial J}{\partial r} \right), \\ \frac{\partial^2\eta}{\partial\phi^2} &= \frac{\sin(2\eta)}{4h_b^4 r^2 J^2} \left( \rho^2 - \rho^2 h_b^4 - 2b^2 h_b^4 + 4\rho b h_b^2 \cos\eta - 4\rho b h_b^4 \cos\eta \right. \\ &\quad \left. - \rho^2 \cos(2\eta) + 2\rho^2 h_b^2 \cos(2\eta) - \rho^2 h_b^4 \cos(2\eta) \right) \\ &\quad - \frac{\partial J / \partial\phi}{2rJ^2} \left( 2 \cos\eta (b + \rho \cos\eta) + 2\rho \sin\eta h_b^{-2} \right), \\ \frac{\partial J}{\partial\phi} &= \frac{\rho^3 b (1 - h^2) \sin\eta}{J h_b^3 r^4} + \frac{\rho \sin\eta}{2J h_b^5 r^4} \left( b h_b^2 - \rho \cos\eta + \rho h_b^2 \cos\eta \right) \\ &\quad \times \left( \rho^2 + \rho^2 h_b^2 + 2b^2 h_b^2 h_b^2 + 2\rho b h_b^2 \cos\eta + 2\rho b h^2 h_b^2 \cos\eta \right. \\ &\quad \left. - \rho^2 \cos(2\eta) + \rho^2 h_b^2 \cos(2\eta) \right), \end{aligned}$$

$$\begin{aligned}
\frac{\partial J}{\partial r} = & \frac{-3\rho}{2h_b^3 r^4} (\rho^2 + \rho^2 h_b^2 + 2b^2 h^2 h_b^2) \\
& + 2\rho b h_b^2 \cos \eta + 2\rho b h^2 h_b^2 \cos \eta - \rho^2 \cos(2\eta) + \rho^2 h_b^2 \cos(2\eta)) \\
& + \frac{\rho (\rho + b h^2 \cos \eta)}{2J h_b^4 r^5} (\rho^2 + \rho^2 h_b^2 + 2b^2 h^2 h_b^2 + 2\rho b h_b^2 \cos \eta \\
& + 2\rho b h^2 h_b^2 \cos \eta - \rho^2 \cos(2\eta) + \rho^2 h_b^2 \cos(2\eta)) \\
& + \frac{\rho}{J h_b^4 r^5} (\rho^3 + \rho^3 h_b^2 + \rho b^2 h^2 h_b^2 + \rho b^2 h^4 h_b^2 + 2b^2 J \varepsilon^2 h_b^3 r^3 \\
& + \rho^2 b h_b^2 \cos \eta + 3\rho^2 b h^2 h_b^2 \cos \eta + 2\rho b J \varepsilon^2 h_b^3 r^3 \cos \eta \\
& - \rho^3 \cos(2\eta) + \rho^3 h_b^2 \cos(2\eta)) .
\end{aligned}$$

## REFERENCES

- ARNOLD, V. I. 1983 *Geometrical Methods in the Theory of Ordinary Differential Equations*. Springer.
- BATCHELOR, G. K. 1956 On steady laminar flow with closed streamlines. *J. Fluid Mech.* **1**, 177–190.
- BERGER, S. A., TALBOT, L. & YAO, L. S. 1983 Flow in curved pipes. *Ann. Rev. Fluid Mech.* **15**, 461–512.
- CARO, C. G., DOORLY, D. J., TARNAWSKI, M., SCOTT, K. T., LONG, Q. & DUMOULIN, C. L. 1996 Non-planar curvature and branching of arteries and non-planar-type of flow. *Proc. R. Soc. Lond. A* **452**, 185–197.
- CARO, C. G., FITZ-GERALD, J. M. & SCHROTER, R. C. 1971 Atheroma and arterial wall shear: Observation, correlation and proposal of a shear dependent mass transfer mechanism of atherogenesis. *Proc. R. Soc. Lond. B* **177**, 109–159.
- CHANDRAN, K. B. 1993 Flow dynamics in the human aorta. *J. Biomech. Engng* **115**, 611–616.
- CHENG, K. C. & MOK, S. Y. 1986 In *Fluid Control and Measurement*, vol. 2 (ed M. Harara), pp. 765–773. Pergamon.
- CHILDRESS, S., LANDMAN, M. & STRAUSS, H. 1989 Steady motion with helical symmetry at large Reynolds number. In *Proc. IUTAM Symp. on Topological Fluid dynamics* (ed. H. K. Moffatt & A. Tsinober), pp. 216–224. Cambridge University Press.
- COLLINS, W. M. & DENNIS, S. C. R. 1975 The steady motion of a viscous fluid in a curved tube. *Q. J. Mech. Appl. Maths* **28**, 133–56.
- DASKOPOULOS, P. & LENHOFF, A. M. 1989 Flow in curved ducts: bifurcation structure for stationary ducts. *J. Fluid Mech.* **203**, 125–148.
- DEAN, W. R. 1927 Note on the motion of fluid in a curved pipe. *Phil. Mag.* **4**, 208–223.
- DEAN, W. R. 1928 The streamline motion of fluid in a curved pipe. *Phil. Mag.* **5**, 673–695.
- DENNIS, S. C. R. & NG, M. 1982 Dual solutions for steady laminar flow through a curved pipe. *Q. J. Mech. Appl. Maths* **35**, 305–324.
- DENNIS, C. R. & RILEY, N. 1991 On the fully developed flow in a curved pipe at large Dean number. *Proc. R. Soc. Lond. A* **434**, 473–478.
- DRITSCHEL, D. G. 1991 Generalised helical Beltrami flows in hydrodynamics and magnetohydrodynamics. *J. Fluid Mech.* **222**, 525–541.
- FLETCHER, C. A. J. 1991 *Computational Techniques in Fluid Dynamics*. Springer.
- GAMMACK, D. & HYDON, P. E. 1998 Steady flow in pipes of non-uniform curvature and torsion. *J. Fluid Mech.* (submitted)
- GERMANO, M. 1982 On the effect of torsion in a helical pipe flow. *J. Fluid Mech.* **125**, 1–8.
- GERMANO, M. 1989 The Dean equations extended to a helical pipe flow. *J. Fluid Mech.* **203**, 289–305.
- GIDDENS, D. P., ZARINS, C. K. & GLAGOV, S. 1993 The role of fluid mechanics in the localization and detection of atherosclerosis. *J. Biomech. Engng* **115**, 588–594.
- KAO, H. C. 1987 Torsion effects on fully developed flow in a helical pipe. *J. Fluid Mech.* **184**, 335–356.
- LANDMAN, M. 1990 Time dependent helical waves in rotating pipe flow. *J. Fluid Mech.* **221**, 289–310.

- LIU, S. & MASLIYAH, J. 1993 Axially invariant laminar flow in helical pipes with finite pitch. *J. Fluid Mech.* **251**, 315–353.
- MCDONALD, D. A. 1974 *Blood Flow in Arteries*. Southampton: The Camelot Press Ltd.
- MAHALOV, A., TITI, E. S. & LEIBOVICH, S. 1990 Invariant helical subspaces for the Navier–Stokes equations. *Arch. Rat. Mech. Anal.* **112**, 193–222.
- MASAWA, N., GLAGOV, S. & ZARINS, C. K. 1994 Quantitative morphological study of intimal thickening at the human carotid bifurcation. *Atherosclerosis* **107**, 137–146.
- PEDLEY, T. J. 1980 *The Fluid Mechanics of Large Blood Vessels*. Cambridge University Press.
- PEDLEY, T. J. 1995 High Reynolds number flow in tubes of complex geometry with application to wall shear stress in arteries. In *Biological Fluid Dynamics, 49th SEB Symposium*. The Society for Experimental Biology.
- SMITH, F. T. 1976 Steady motion in a curved pipe. *Proc. R. Soc. Lond. A* **347**, 345–370.
- STRIKWERDA, J. C. 1989 *Finite Difference Schemes and Partial Differential Equations*. Wadsworth & Brooks/Cole.
- TUTTLE, E. R. 1990 Laminar flow in twisted pipes. *J. Fluid Mech.* **219**, 545–570.
- YANASE, S., GOTO, N. & YAMAMOTO, K. 1989 Dual solutions of the flow through a curved tube. *Fluid Dyn. Res.* **5**, 191–201.
- ZABIELSKI, L. 1996 Helical pipe flows in haemodynamics. PhD thesis, Imperial College, London.
- ZABIELSKI, L. & MESTEL, A. J. 1998 Unsteady blood flow in a helical pipe. *J. Fluid Mech.* **370**, 321–345 (referred to herein as ZM2).